Thermal Characteristics of Mirror-Based Optical Redistribution for Co-Packaged Optics

Fumi Nakamura, *Member, IEEE*, Satoshi Suda, Takayuki Kurosu, *Member, IEEE*, Yasuhiro Ibusuki, Akihiro Noriki, Akio Ukita, Koichi Takemura, *Member, IEEE*, Tsuyoshi Aoki, and Takeru Amano

***Abstract*—Because traffic toward and inside datacenters is increasing, the power consumption of electrical wiring in ethernet switches for datacenter should be addressed. Co-packaged optics (CPO) is a promising solution, where optical components are integrated into the same package substrate as electrical elements. We have proposed one of the CPO modules, where micro-mirror- based optical redistribution is adopted for low-loss and broadband optical coupling. CPO is required to operate at high temperatures; however, this redistribution uses materials with different coefficients of thermal expansion; thus, there is concern about its operation. In this study, the thermo-optical characteristics in the C-band were analyzed by the finite element method for thermal deformation and physical optical propagation analysis. The coupling efficiency of more than 85% was obtained at 1550 nm in the specified temperature range of 15–85 °C, and the difference in the average coupling loss between 20 °C and 85 °C was 0.49 dB in the calculation. The temperature-dependent transmittance was experimentally demonstrated using fabricated optical redistribution, and the average loss difference in C-band was 0.80 dB at 25 °C, 55 °C, and 85 °C.**

***Index Terms*—Co-packaged optics, datacenter, polymer waveguide, silicon photonics, thermal analysis.**

I. Introduction

DATACENTER IP traffic is rapidly increasing, driven by the growth of cloud computing and applications, such as video streaming and the Internet of Things [1]. The bandwidth of switch application-specific integrated circuits (ASIC), which process signals in datacenter networks, also increases yearly. It achieved 25.6 Tb/s in 2019 according to Broadcom [2], and it is expected to reach 51.2 Tb/s in a few years [3]. In optical interconnections in datacenter networks, based on pluggable transceivers, signals are processed, transferred electrically, and converted to optical signals at the edge of a printed circuit board (PCB). Although pluggable optics continue to work for scaled-up data centers, the transmission capacity will be limited because of the power consumption of the electrical path in the future. To address this bottleneck, co-packaged optics (CPO), in which electrical and optical components are integrated on a package substrate, has been proposed [4], [5], [6]. In CPO, electrical signals are converted by optical transceiver chips near electrical processors, such as ASIC, on the substrate, and parts of the electrical wires can be substituted by a low-power consumptive optical link. CPO modules and related technologies have been extensively developed for realizing CPO in the path over 51.2 Tb/s, CPO modules and related technologies are extensively developing [7], [8], [9], [10], [11]. Furthermore, high-functional CPOs using matured C-band-based components in silicon photonics are also being researched for next-generation datacenter architectures in advance of O-band [12], [13]. A next-generation CPO configuration is required for future packaging beyond 100 Tb/s ASIC, where optics are integrated close to electrical components [3].

To meet this demand. we have recently proposed one of CPO configurations, which is named active optical package (AOP) substrate [14], [15], where silicon photonics chip is embedded on the packaged substrate and electrical components can be integrated close to optics. In the AOP, polymer waveguides are used as optical links on the substrate, and optical connection between silicon photonics and a polymer waveguide are required. Some coupling technologies have been developed for silicon photonics, such as spot size converters [16], grating couplers [17], and adiabatic couplers [18]. For achieving low-loss broadband optical coupling, 3D micro-mirror-based optical redistribution has been developed in the AOP [14].

Considering the practical use of CPO modules in datacenters and network nodes, assuming their operation at high temperatures is necessary. The proposed optical redistribution comprises silicon, silica, polyimide, polymer cladding, and a polymer core, where the stacked materials have more than two order difference in the coefficient of thermal expansion (CTE). Therefore, at high temperatures, the difference in thermal deformation between the elements affects the coupling efficiency. According to the 3.2 Tb/s CPO optical module product requirements document issued in 2021 by CPO collaboration, operating temperature in case of integrated laser is from 15 °C to 70 °C, and that in case of external laser is from 15 °C to 85 °C [19]. Following this specification, the CPO module requires the ability to operate

Manuscript received 19 March 2023; revised 23 May 2023; accepted 29 May 2023. Date of publication 5 June 2023; date of current version 2 October 2023. This work was supported by New Energy and Industrial Technology Development Organization (NEDO) under Grant JPNP13004. *(Corresponding author: Fumi Nakamura.)*

Fumi Nakamura, Satoshi Suda, Takayuki Kurosu, Akihiro Noriki, and Takeru Amano are with the National Institute of Advanced Industrial Science and Technology (AIST), Tsukuba, Ibaraki 305-8568, Japan, and also with the Photonics Electronics Technology Research Association (PETRA), Tsukuba, Ibaraki 305-8569, Japan (e-mail: fumi.nakamura@aist.go.jp; s-suda@aist.go.jp; t.kurosu@aist.go.jp; a-noriki@aist.go.jp; takeru-amano@aist.go.jp).

Yasuhiro Ibusuki, Akio Ukita, Koichi Takemura, and Tsuyoshi Aoki are with the Photonics Electronics Technology Research Association (PETRA), Tsukuba 305-8569, Japan (e-mail: yasuhiro.ibusuki@furukawaelectric.com; a-ukita@nec.com; k-takemura@aiocore.com; aoki-t@fujitsu.com).

Color versions of one or more figures in this article are available at https://doi.org/10.1109/JLT.2023.3283023.

Digital Object Identifier 10.1109/JLT.2023.3283023

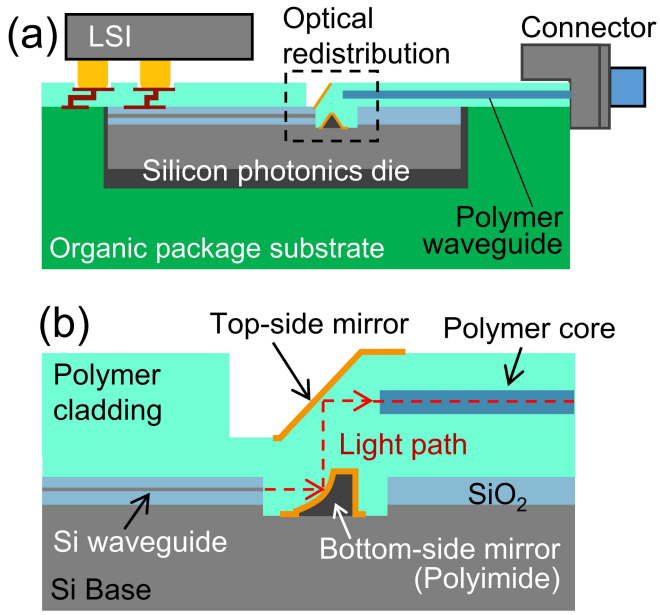

Fig. 1. Schematics of the active optical package (AOP) substrate: (a) Cross-section view, (b) enlarged view of a micro-mirror-based optical redistribution.

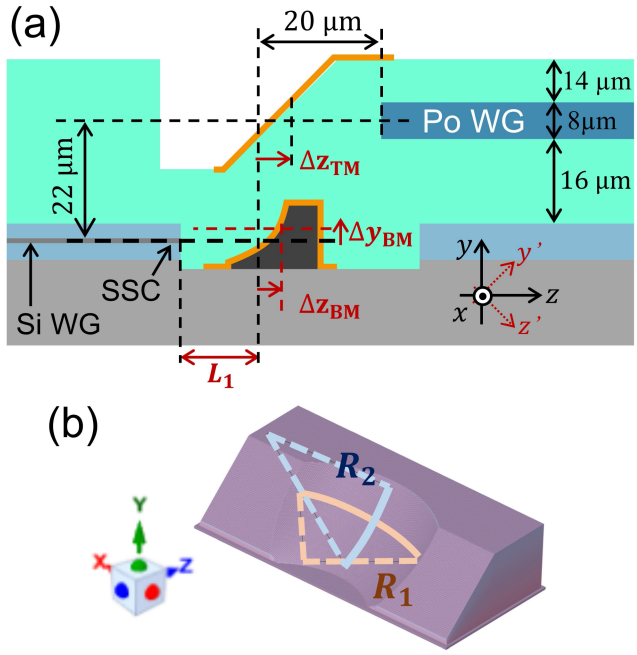

Fig. 2. Design parameters for optimization of (a) optical redistribution, (b) bottom-side mirror.

from 15 °C to 85 °C. The low-loss transmittance of the optical redistribution at room temperature has been confirmed so far [14], [15]; however, the temperature-dependent characteristics have not been sufficiently verified yet.

In this study, the micro-mirror-based optical redistribution's thermal characteristics are calculated numerically and demonstrated experimentally with a fabricated device-under-test (DUT) sample in the C-band. In Section II, optical re-distribution is designed at wavelength 1550 nm, and then the temperature-dependent coupling efficiency of the designed redistribution is calculated by thermal deformation using the finite element method and physical optics propagation analysis in Section III. The cause of coupling loss caused by temperature variation is also discussed. In Section IV, the transmittance of the fabricated device is demonstrated at high temperatures. Although some of the results have been briefly reported in previous conference abstracts [20], [21], the details of the design and analysis method of optical redistribution and discussions about the cause of loss increment at high temperatures are additionally included herein. In addition, based on discussion of the cause of temperature-dependent loss in analysis, the redesign was proposed at operating temperature. The results of the analysis and experiment are concluded in Section V.

II. Structure of Micro-Mirror-Based Optical Redistribution

A. Schematic of Optical Redistribution

Fig. 1 shows a schematic of the active optical package (AOP) substrate [14]. As shown in Fig. 1(a) cross section of the AOP, silicon photonic die embedded in an organic package substrate, and polymer waveguides integrated to link the optical elements on the board. A micro-mirror-based optical redistribution is adopted in Fig. 1 as a coupling between the silicon photonics and polymer waveguides. (b). It consists of a silicon waveguide, polymer waveguide, and a pair of 3D micro-mirrors. The top-side mirror has a linearly angled surface, and the bottom-side mirror is curved to convert the spot size from the silicon waveguide to the polymer waveguide. Using a 3D micro-mirror, broadband, low-loss, and polarization-diverse optical coupling can be obtained.

B. Optimizing Design at Room Temperature

Before calculating the thermal characteristics, the design parameters of the optical redistribution are optimized at room temperature, 20 °C, and then propagated using optical propagation analysis with commercial optical software *Zemax OpticStudio (ver.22.3)*. The wavelength of the calculation was 1550 nm in the C band. The design details and parameters of the optical redistribution for optimization are shown in Fig. 2. The top-side mirror has a 45-degree tilted mirror surface and the height difference between the silicon waveguide and the polymer waveguide is set to 22 µm. The bottom-side mirror is defined as a biconic surface with curvature R_1 on the x-axis and R_2 on the y-axis. Thereafter, it is tilted 45° about the x-axis, as the axis y' and z' in Fig. 2(b).

The curvatures of bottom-side mirror R_1 and R_2, the distance between the silicon waveguide to the bottom-side mirror L_1, decentering parameters for the bottom-side mirror at y-axis direction Δy_{BM}, at z-axis Δz_{BM}, and a parameter for the top-side mirror at z-axis direction Δz_{TM} are optimized by the damped least square method, to obtain the maximum coupling efficiency from silicon waveguide to polymer waveguide at room temperature. There is an inversed-taper spot-size converter (SSC) at the edge of the silicon waveguide for emitting toward the bottom-side mirror. The optical beams from the SSC

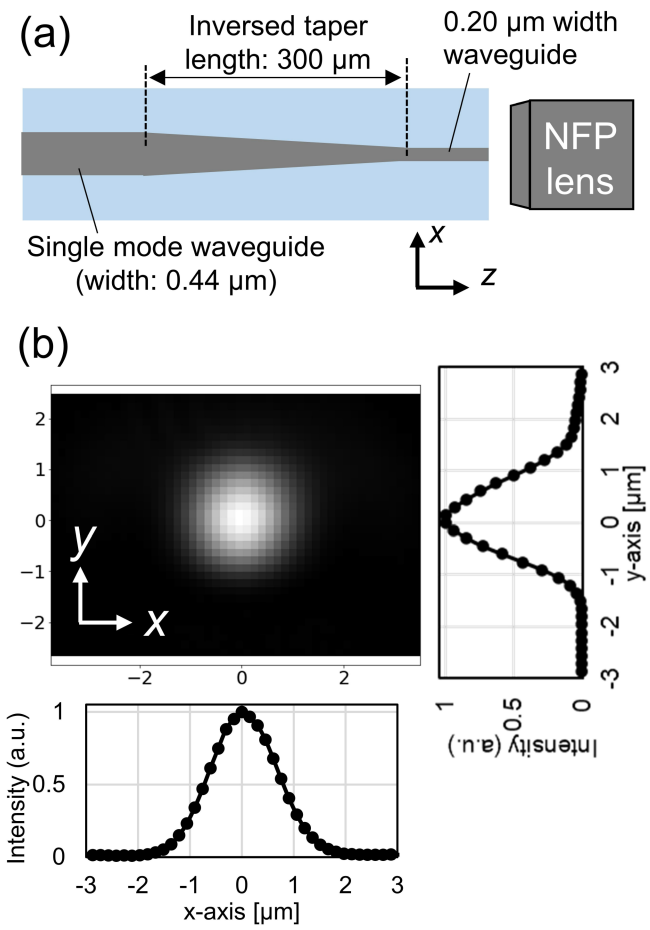

Fig. 3. Measurement of near field pattern (NFP) of beam emitted from SSC. (a) Top-view of measured SSC, and (b) measured NFP of TE -mode and its line profiles.

are represented as a Gaussian beam, whose beam waists were obtained by near field pattern (NFP) measurement of SSC as shown in Fig. 3. Fig. 3(a) shows the top view of the design of measured SSC, and Fig. 3(b) shows measured NFP and line profiles of TE mode. The beam waist emitted from SSC was set to 1.33 μm at the *x*-axis and 1.34 μm at the *y*-axis, as obtained by the Gaussian fitting of the measurement result. The mode-field diameter (MFD) of the polymer waveguide was set to 10.4 μm. This value came from MFD of standard single mode fiber (SMF), such as Corning SMF-28 [22], since polymer waveguide connects to the SMF of the optical connector at the edge of the substrate as shown in Fig. 1(a), and it is designed and fabricated to suited to MFD of SMF. Optimized design parameter values are shown in Table I. The coupling efficiency was 95.7% for the optimized parameters.

III. Analyzing Thermal Deformation and Optical Characteristic

In this section, the thermal deformation and optical characteristics of the optical redistributions as well as the designed values in the previous section are analyzed. First, the thermal deformations were calculated using *ANSYS Mechanical*, and

TABLE I
Optimized Parameter Values of Optical Redistribution at Room Temperature

Design Parameter	Symbol	Value [μm]
Length between silicon waveguide and bottom-side mirror	L_1	20.35
Curvature of bottom-side mirror in *x*-axis	R_1	28.67
Curvature of bottom-side mirror in *y*'-axis	R_2	57.41
Decentering parameter of bottom-side mirror at *y*-axis	Δy_{BM}	0.15
Decentering parameter of bottom-side mirror at *z*-axis	Δz_{BM}	1.23
Decentering parameter of top-side mirror at *z*-axis	Δz_{TM}	0.34

then the deformed mirrors were fitted with a 2-dimensional polynomial to be imported into the optical software. Finally, the temperature-dependent optical coupling efficiency of the optical redistribution was analyzed using the mirror surface defined using the fitting results.

A. Analyzing Thermal Deformation

In the first step, 3D computer-aided design (CAD) models of redistribution were prepared using the design parameters described in Section 2.2. Herein, the center of the silicon waveguide facet was set at the origin of *xyz* coordinates. Thermal deformations were calculated using the commercial finite element analysis software *ANSYS Mechanical*. The analyzed horizontal range was 500 μm by 500 μm at *zx*-dimension. The thicknesses of the Si base, a buried oxide (BOX) layer, and SiO_2 overcladding were set to 775 μm, 2.99 μm, and 1.89 μm, respectively. The thickness of polymer under cladding and over cladding is 8 μm and 12 μm as shown in Fig. 2(a). The core size of the polymer waveguide is set to be 8 μm × 8 μm, and the core height and width of the silicon waveguide are defined to be 0.22 μm and 0.50 μm in the thermal analysis 3D model. The bottom of the Si base was fixed as a boundary condition. It is defined that the temperature of all components is uniform and the temperature range is from −35 °C to 200 °C. The reference temperature is set to 20 °C. The materials used for elements of optical redistribution are shown in Fig. 1(b). The bottom-side mirror was made of polyimide, and the top-side mirror was made of polymer cladding. The thermal properties of the materials comprising the optical redistribution are listed in Table II. Si was assumed to exhibit orthotropic properties [24]. The top surface of the Si wafer was in the <100> direction. The axes of the table are shown in Fig. 2(a).

The results of the thermal deformation analysis of the optical redistribution are shown in Fig. 4. Fig. 4(a) shows the maximum displacement from the position at room temperature of 20 °C at each element for the optical redistribution. The surfaces of the bottom- and top-side mirrors and the end facets of the silicon and polymer waveguides were evaluated. The maximum total deformation at 85 °C of silicon waveguide, bottom-side mirror, polymer waveguide, and top-side mirror was 0.14 μm, 0.25 μm, 0.87 μm, and 1.16 μm, respectively. To make the thermal deformation in the *y*- and *z*- axis visible, Fig. 4(b) shows

TABLE II
THERMAL PROPERTY OF MATERIALS COMPOSING OPTICAL REDISTRIBUTION

Material	Young's Modulus [GPa]	Poisson's ratio	Coefficient of thermal expansion [°C $^{-1}$]
Polymer Cladding	0.5 [23]	0.4	1.8×10^{-4} [23]
Polymer Core	1.0 [23]	0.4	1.5×10^{-4} [23]
Polyimide	4.0	0.34	4.0×10^{-5}
Cladding (SiO2)	73	0.155	5.55×10^{-7}
Silicon	169 (x, z) 130 (y) [24]	0.36 (x-y) 0.28 (y-z) 0.064 (z-x) [24]	2.59×10^{-6} [25]

the deformed shape of elements composing optical redistribution in the yz-cross section at 20 °C, 85 °C, and 200 °C. The shapes were obtained by extracting plots at approximately $x = 0$ from the exported 3D CAD file. The polymer cladding and core material have a larger CTE; thus, the top-side mirror and polymer waveguide are more deformed than other elements, such as silicon waveguides and bottom-side mirrors, by changing the temperature. Although the topside mirror and polymer waveguide were made of the same material, the polymer thickness under the topside mirror was larger than that under the polymer waveguide, resulting in a larger deformation.

B. Fitting With 2D Polynomial

The deformed mirror surface was exported from *ANSYS* in the STL CAD format and fitted with a fifth-ordered xy polynomial for import into the optical software *ZEMAX OpticStudio*. This is shown in (1). In the fifth-order polynomial, there are 21 coefficients, including x^0y^0. The fitting range on the x-axis for the top-side mirror is set to ± 10 µm, which is enough range to correspond to the beam size reflected by these mirrors. The y-axis origin of the fitting was set to the center height of the corresponding waveguide, the silicon waveguide for the bottom-side mirror, and the polymer waveguide for the top-side mirror.

$$z = \sum_{i=0}^{5}\sum_{j=0}^{5} a_{ij}x^i y^j \tag{1}$$

At this time, the average root mean squared error (RMSE) with the fitting was less than 1 nm in the bottom-side and 9 nm in the top-side mirror in the range of −35–200 °C. The fitting error of the top-side mirror was larger than that of the bottom-side mirror because the former underwent a larger amount of deformation. The silicon and polymer waveguide deformations were considered in terms of the yz center position.

C. Analyzing Temperature-Dependent Coupling Efficiency

The thermally dependent optical coupling efficiency from the silicon waveguide to the polymer waveguide through the micro-mirrors was calculated using the results of thermal deformation. The thermally deformed mirror surfaces were defined as extended polynomial surfaces with coefficients obtained by

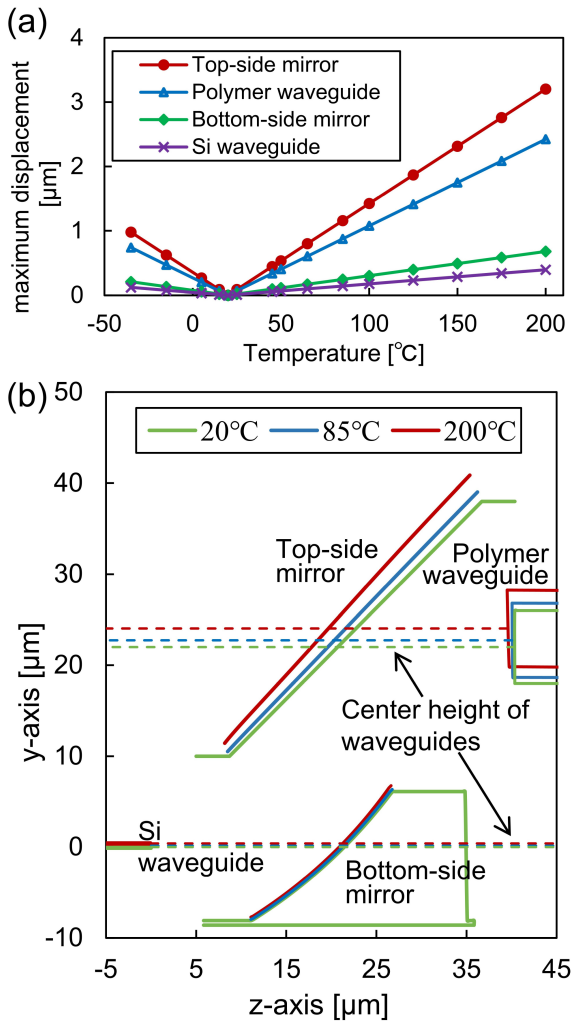

Fig. 4. Result of thermal deformation analysis of optical redistribution (a) the maximum displacement from the position at room temperature at each element. (b) The deformed shape of elements composing optical redistribution at in yz-cross section at 20, 85, 200 °C.

2D fitting in the previous section, and the positions of the waveguides were set to y-z position of waveguides' endfacet after thermal deformation in *Zemax OpticStudio*. The temperature dependence of polymer cladding's refractive index was considered using the thermo-optic coefficient of refractive index of OrmoClad $dn/dT = 2.7 \times 10^{-4}$ K^{-1} [23]. The widths of the Gaussian beam from the silicon waveguide and the MFD of the polymer waveguide were set to be the same as those used in the design optimization described in Section II-B. The results of the analysis of the coupling efficiency considering thermal deformation are shown in Fig. 5. Fig. 5(a) shows the temperature-dependent coupling efficiency of the optical redistribution at a wavelength of 1550 nm. According to the figure, more than 85% coupling efficiency is obtained at wavelength 1550 nm in the operation temperature specification for CPO 15 °C–85 °C. This indicates that the micro-mirror-based optical redistribution has a high thermal tolerance, although materials with different CTE layer it. The design of the analyzed optical redistribution has been optimized for room temperature; therefore,

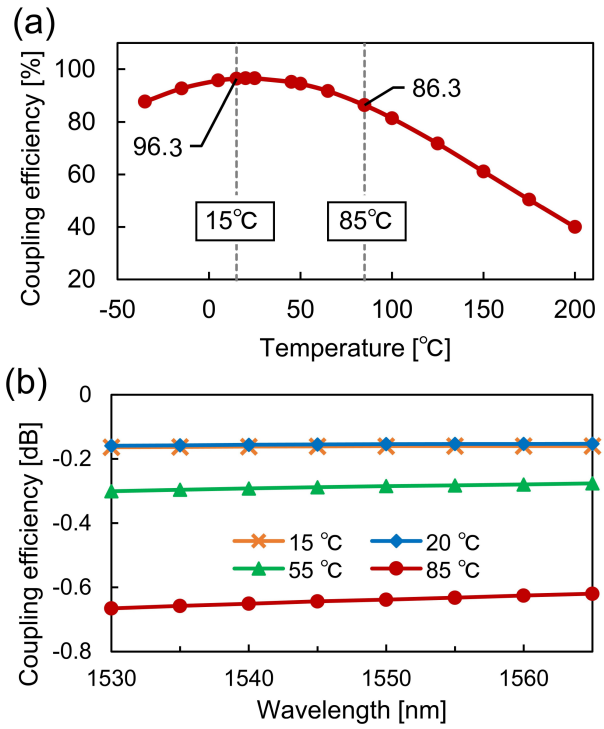

Fig. 5. Result of calculating coupling efficiency considering thermal deformation, (a) calculated temperature-dependent coupling efficiency of optical redistribution in 1550 nm. (b) Coupling efficiency in C-band at 15, 20, 55, and 85 °C.

the coupling efficiency is maximized at around 20 °C. Fig. 5(b) shows the wavelength-dependent coupling efficiency in C-band at 15 °C, 20 °C, 55 °C, and 85 °C. The redistribution shows flat transmission in C-band, and the difference in the average coupling loss between 20 °C and 85 °C is 0.49 dB.

D. Discussion of Calculation Results

To discuss the loss factors at high temperatures, the coupling efficiencies were calculated, where divided parts of thermal deformations at 85 °C were applied. First, the thermal deformations of the silicon waveguide and bottom-side mirror were considered. The coefficient of x_0y_1 in (1) was set to be the same as that at room temperature to exclude the influence of misalignment in the pair of mirrors owing to the changing angle at the bottom-side mirror. The effect of mirror angle change was evaluated separately. The coupling efficiency was 96.5% at 85 °C, and the loss increasement from room temperature was less than 0.001 dB. Thus, the deformations at the silicon waveguide and bottom-side mirror, except for the angle change, slightly affected on the loss increase. Next, the coupling efficiency was calculated using the deformation coefficient of the polymer waveguide and the top-side mirror, whose angle was set to 45°, similar to that at room temperature. The coupling efficiency was 95.9%, and the loss increasement from room temperature was 0.027 dB. Finally, when only the angles of a pair of mirrors were considered using the fitting coefficient of x_0y_1 at 85 °C, the coupling efficiency was 86.4% and the loss increased from 20 °C was 0.479 dB. Based on that the loss is 0.484 dB, where

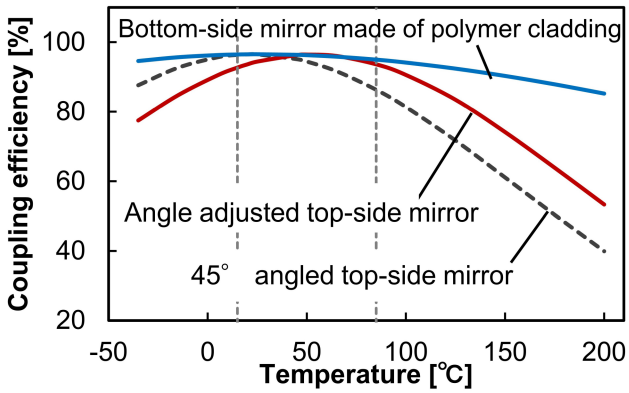

Fig. 6. Calculated temperature-dependent coupling efficiency of optical redistribution using angle adjusted top-side mirror and that using bottom-side mirror made of polymer cladding.

all thermal deformations at 85 °C are considered, it can be observed that the deviation in the angular relationship between the top- and bottom-side mirrors increases coupling loss at high temperatures. Because the angle difference at 85 °C compared with 20 °C is 0.31° at the bottom-side mirror and 0.96° at the top-side mirror, the change in the angle of the top-side mirror made of polymer cladding affects the coupling loss owing to a larger expansion coefficient.

Considering this estimated loss breakdown, the optical redistribution is redesigned for the specified temperature range from 15 °C to 85 °C for CPO. As shown in Fig. 5(a), the coupling efficiency has reached a maximum value at approximately 20 °C, because the parameters have been optimized at room temperature as described in Section II. Therefore, the design is adjusted to ensure that the maximum coupling efficiency is achieved around 50 °C, which is the center of the temperature specification. As described previously, a change in the angle of the micro-mirrors has a significant effect on the efficiency. As the temperature increases, the angle of the topside mirror becomes steeper. By setting the angle of top-side mirror to 44.7° at room temperature to reduce angle mismatch in the temperature range, the coupling is more than 92% in the range of 15–85 °C, as shown in Fig. 6 with a red line. At this time, the angle difference between mirrors is 0.54° at 85 °C, and which 0.84° using a 45-degree-tilted top-side mirror. In addition, because this redistribution is a pair of mirrors, if the angle of the bottom-side mirror changes similarly to that of the top-side mirror, it compensates for the misalignment caused by angle deformation. Therefore, by using polymer cladding material to bottom-side mirror as same as the top-side mirror, the thermal characteristics become flat, and a coupling efficiency of more than 94% can be obtained at 15–85 °C as shown in Fig. 6 with a blue line. The maximum angle difference between mirrors is 0.22° at 15–85 °C, and the angle mismatch is suppressed by composing the mirrors with the same material.

IV. Experiment

The thermal characteristics of the C-band were demonstrated using a silicon photonic die with optical redistribution, as shown

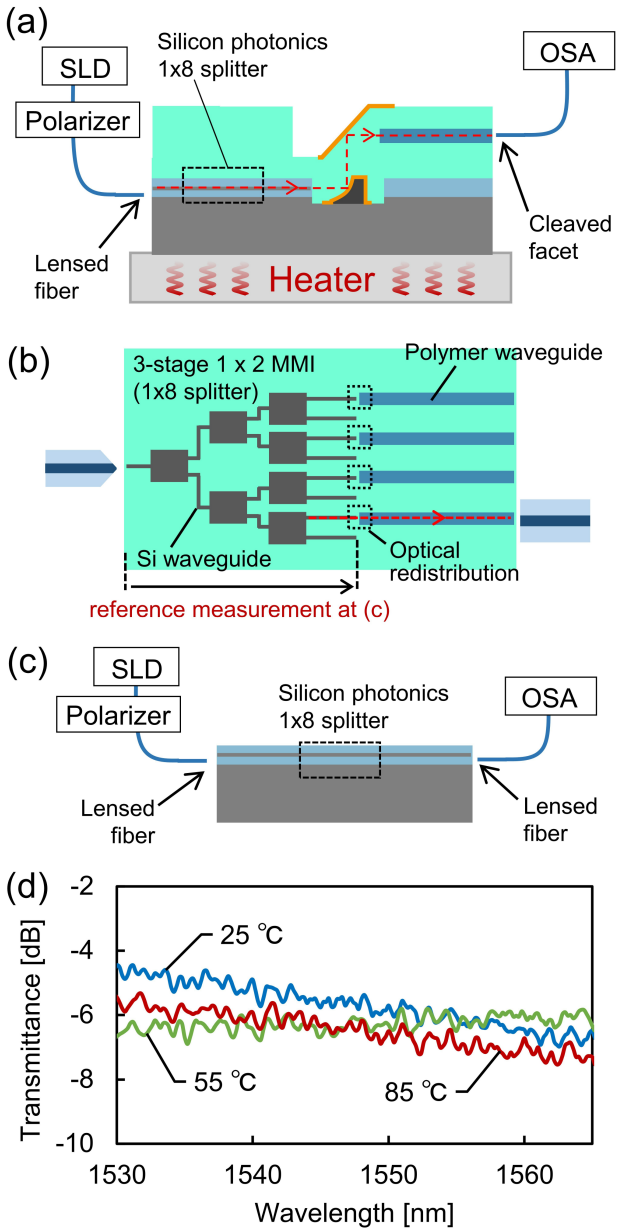

Fig. 7. Demonstration of thermal characteristics of a device-under-test (DUT) sample including optical redistribution. (a) Setup for evaluation of thermal characteristics with DUT, (b) top-side view of schematic of DUT, (c) setup for reference transmittance, (d) measured transmittance of optical redistribution in C-band at 25 °C (room temperature), 55 °C, and 85 °C, obtaining by subtracting the reference transmittance of silicon waveguide from the measured transmittance of DUT.

in Fig. 7. In this DUT sample, the parameter value was designed for room temperature, and the bottom mirror was made of a photosensitive polyimide. The 3D top- and bottom-side mirrors were formed using UV grayscale lithography, and the polymer layers were patterned using laser lithography. The details of the fabricated DUT sample with optical redistribution are explained in a previous study [14]. The setup for measuring the thermal characteristics of the DUT is shown in Fig. 7(a). Broadband light from a superluminescent diode (SLD) source was inserted into a silicon waveguide of the DUT via a spherical lensed fiber after being polarized to the TE mode. Then it propagated through mirror-based optical redistribution, and the light was emitted from the polymer waveguide to a single-mode (SM) fiber with a cleaved facet. Its transmittance was measured using an optical spectrum analyzer (OSA). The DUT silicon die was heated from below. The silicon photonic parts in the DUT have a 1×8 splitter composed of 3-stage 1×2 multimode interferences (MMI) as shown in Fig. 7(b). The splitter is integrated for convenience of measurements because it allows evaluation of multiple optical redistributions without re-aligning between the silicon waveguide and lensed fiber. Four of the eight outputs were connected to polymer waveguides with each redistribution in the DUT, while four were left open. In the measurement, the temperature characteristics were evaluated in the path, where the highest coupling efficiency was obtained at room temperature among the four paths. For excepting insertion loss of 1×8 splitter from the DUT measurement result, the reference transmittance was measured as shown in Fig. 7(c). The reference device, including a 1×8 splitter with SSCs on both sides, was cut out from a silicon photonics die whose design is the same as the chip used in the DUT. In the reference measurements, spherical lensed fibers were used for the input and output of the silicon waveguide because their MFD was smaller than those of a fiber and a polymer waveguide.

The transmittance of optical redistribution in the C-band where the wavelength is between 1530 nm and 1565 nm, at room temperature 25 °C, 55 °C, and 85 °C, is shown in Fig. 7(d). This is obtained by subtracting the measured reference transmittance of the silicon waveguide at room temperature from the measured transmittance of the DUT sample. The average insertion loss in C-band is 5.63 dB, 6.26 dB, and 6.43 dB at temperature 25 °C, 55 °C, and 85 °C, respectively. The measurement values include the propagation loss of a 5.0 mm-length polymer waveguide, which is 0.49 dB on average at room temperature and its thermally dependent loss, as well as the coupling loss from the silicon waveguide to the polymer waveguide via micro-mirrors. The average loss difference is only 0.80 dB among 25 °C, 55 °C, and 85 °C; low temperature-dependent characteristics of optical redistribution were demonstrated as same as calculation in the previous Section III, even the measured temperature dependence includes propagation loss difference at polymer waveguide and silicon waveguide. The measured coupling loss of the DUT is larger than that of the calculation owing to the mode mismatch and misalignment caused by fabrication error. As discussed in [14], coupling efficiency can be increased by improving fabrication misalignment.

These results verified the temperature stability of optical redistribution in the experiment, not only in the analysis. The redistribution works stable at 15–85 °C, the external-laser type CPO specification. Using optical redistribution and silicon photonics dies, where temperature-stable quantum dot lasers are mounted [26], [27], laser-integrated CPO beyond the specified operating temperature (15–70 °C for laser-mounted type CPO) can be expected in the future.

V. Conclusion

The thermal characteristics of the optical redistribution of the CPO, which consists of silicon photonics, a polymer waveguide,

and a pair of micro-mirrors, were analyzed numerically and demonstrated experimentally using a fabricated sample in the C-band. The calculated coupling efficiency was more than 85% at 1550 nm in the range 15–85 °C, where CPO was required to operate. The breakdown of the temperature-dependent loss was discussed, and it was found that the angle mismatch of the mirrors increased the coupling loss at high temperatures. The coupling efficiency of over 90% was obtained at 15–85 °C by adjusting the angle of the top mirror to 44.7°. Additionally, it was found that flatter thermal characteristics could be obtained by unifying the materials of the top- and bottom-side mirrors. The results obtained in these analyses are expected to support the properties of the redistribution designed for the O-band. Fabricated DUT's temperature-dependent transmission loss difference was 0.80 dB at 25 °C, 55 °C, and 85 °C. The low temperature-dependent characteristics were confirmed both numerically and experimentally. A broadband and high thermal tolerant optical connection can be obtained on the CPO substrate using mirror-based optical redistribution.

REFERENCES

[1] Cisco, "Cisco global cloud index: Forecast and methodology 2016–2021," White Paper, San Jose, CA, USA, 2018.

[2] Broadcom, "Broadcom ships tomahawk 4, industry's highest bandwidth ethernet switch chip at 25.6 terabits per second," 2019. Accessed: Mar. 2, 2023. [Online]. Available: https://www.broadcom.com/company/news/product-releases/52756

[3] C. Minkenberg, R. Krishnaswamy, A. Zilkie, and D. Nelson, "Co-packaged datacenter optics: Opportunities and challenges," *Inst. Eng. Technol. Optoelectron.*, vol. 15, no. 2, pp. 77–91, Mar. 2021, doi: 10.1049/ote2.12020.

[4] N. Margalit et al., "Perspective on the future of silicon photonics and electronics," *Appl. Phys. Lett.*, vol. 118, no. 22, pp. 1–10, May 2021, doi: 10.1063/5.0050117.

[5] R. Stone et al., "Co-packaged optics for data center switching," in *Proc. Eur. Conf. Opt. Commun.*, 2020, pp. 1–3, doi: 10.1109/ECOC48923.2020.9333175.

[6] Co-packaged Optics Collaboration, "Microsoft and Facebook announce formation of the co-packaged optics collaboration under the joint development foundation," 2019. Accessed: Mar. 2, 2023. [Online]. Available: http://www.copackagedoptics.com/2019/06/21/cpo-site/

[7] S. Fathololoumi et al., "1.6Tbps silicon photonics integrated circuit for co-packaged optical-IO switch applications," in *Proc. Opt. Fiber Commun. Conf. Exhib.*, 2020, pp. 1–3.

[8] J. E. Johnson, K. Bacher, R. Schaevitz, and V. Raghunathan, "Performance and reliability of advanced CW lasers for silicon photonics applications," in *Proc. Opt. Fiber Commun. Conf. Exhib.*, 2022, pp. 1–27.

[9] D. Kuchta et al., "Multi-wavelength optical transceivers integrated on node (MOTION)," in *Proc. Opt. Fiber Commun. Conf. Exhib.*, 2019, pp. 1–3.

[10] L. Brusberg, A. R. Zakharian, S. E. Kocabas, J. R. Grenier, C. C. Terwilliger, and A. F. Evans, "Optoelectronic glass substrates for co-packaging of optics and ASICs," in *Proc. Opt. Fiber Commun. Conf. Exhib.*, 2020, pp. 1–3.

[11] Ranovus, "Ranovus demonstrates industry's first adaptive compute acceleration co-packaged optics platform with Xilinx Versal and Ranovus Odin^{TM} 800Gbps CPO 2.0," 2022. Accessed: Mar. 2, 2023. [Online]. Available: https://ranovus.com/ranovus-with-amd-cpo/

[12] M. Glick et al., "PINE: Photonic integrated networked energy efficient datacenters (ENLITENED program) [invited]," *J. Opt. Commun. Netw.*, vol. 12, no. 12, pp. 443–456, Dec. 2020, doi: 10.1364/JOCN.402788.

[13] V. Gopal et al., "Simultaneous error-free data modulation with silicon microdisks in the multi-FSR regime for scalable DWDM links," in *Proc. Opt. Fiber Commun. Conf.*, 2023, pp. 1–3.

[14] A. Noriki et al., "Characterization of optical redistribution loss developed for co-packaged optics," *IEEE Photon. Technol. Lett.*, vol. 34, no. 17, pp. 899–902, Sep. 2022, doi: 10.1109/LPT.2022.3191645.

[15] A. Noriki et al., "Demonstration of silicon-photonics hybrid glass-epoxy substrate for co-packaged optics," in *Proc. Eur. Conf. Opt. Commun.*, 2022, pp. 1–4.

[16] T. Shoji, T. Tsuchizawa, T. Watanabe, K. Yamada, and H. Morita, "Spot-size converter for low-loss coupling between 0.3-/spl mu/m-square Si wire waveguides and single-mode fibers," in *Proc. IEEE 15th Annu. Meeting Lasers Electro-Opt. Soc.*, 2002, vol. 1, pp. 289–290, doi: 10.1109/LEOS.2002.1134041.

[17] D. Taillaert, P. Bienstman, and R. Baets, "Compact efficient broadband grating coupler for silicon-on-insulator waveguides," *Opt. Lett.*, vol. 29, no. 23, pp. 2749–2751, Dec. 2004, doi: 10.1364/OL.29.002749.

[18] R. Dangel et al., "Polymer waveguides enabling scalable low-loss adiabatic optical coupling for silicon photonics," *IEEE J. Sel. Topics Quantum Electron.*, vol. 24, no. 4, Jul./Aug. 2018, Art. no. 8200211, doi: 10.1109/JSTQE.2018.2812603.

[19] Co-Packaged Optics Collaboration, "Development forum releases 3.2T optical module PRD," 2021. Accessed: Jun. 3, 2022. [Online]. Available: http://www.copackagedoptics.com/2021/02/12/development-forum-releases-3-2t-optical-module-prd/

[20] S. Suda et al., "Heat-tolerant 112-Gb/s PAM4 transmission using active optical package substrate for silicon photonics co-packaging," in *Proc. Opto-Electron. Commun. Conf.*, 2021, pp. 1–3.

[21] F. Nakamura et al., "Analyzing thermal tolerance of mirror-based optical redistribution for co-packaged optics," in *Proc. Conf. Lasers Electro-Opt.*, 2022, pp. 1–2.

[22] Corning, "Corning SMF-28 ultra and SMF-28 ultra 200 single-mode optical fibers," Accessed: May 13, 2023. [Online]. Available: https://www.corning.com/optical-communications/worldwide/en/home/products/fiber/optical-fiber-products/smf-28-ultra.html

[23] Micro resist technology, "OrmoCore and OrmoClad," Accessed: Mar. 2, 2023. [Online]. Available: https://www.microresist.de/en/produkt/ormocore-and-ormoclad/

[24] M. A. Hopcroft, W. D. Nix, and T. W. Kenny, "What is the young's modulus of silicon?," *J. Microelectromech. Syst.*, vol. 19, no. 2, pp. 229–238, Apr. 2010, doi: 10.1109/JMEMS.2009.2039697.

[25] Y. Okada and Y. Tokumaru, "Precise determination of lattice parameter and thermal expansion coefficient of silicon between 300 and 1500 K," *J. Appl. Phys.*, vol. 56, no. 2, pp. 314–320, Feb. 1984, doi: 10.1063/1.333965.

[26] Y. Arakawa, T. Nakamura, and J. Kwoen, "Chapter three-quantum dot lasers for silicon photonics," *Semicond. Semimetals*, vol. 101, pp. 91–138, Jul. 2019, doi: 10.1016/bs.semsem.2019.07.007.

[27] Z. Zhou et al., "Prospects and applications of on-chip lasers," *Elight*, vol. 3, no. 1, pp. 1–25, Jan. 2023, doi: 10.1186/s43593-022-00027-x.

Fumi Nakamura (Member, IEEE) received the B.S., M.S., and Ph.D. degrees in electronic and electrical engineering from Keio University, Tokyo, Japan, in 2017, 2018, and 2021, respectively. Since 2021, she has been with the National Institute of Advanced Industrial Science and Technology, Tsukuba, Japan. Her research focuses on co-packaged optics technologies using silicon photonics.

Satoshi Suda was born in Kobe, Japan in 1979. He received the B.S., M.S., and Ph.D. degrees in science and engineering from the Tokyo Institute of Technology, Yokohama, Japan, in 2003, 2004, and 2008, respectively. His Ph.D. thesis involved studies on optical nonlinear devices based on a vertical cavity surface emitting laser at the telecommunication wavelength. In 2008, he joined AIST, where he has been engaged in the research on silicon photonic circuits.

Takayuki Kurosu (Member, IEEE) was born in Japan in 1964. He received the Ph.D. degrees in engineering physics from the University of Tokyo, Tokyo, Japan. In 1991, he joined the National Institute of Advanced Industrial Science and Technology (AIST), Tsukuba, Japan. He built the first Cs atomic fountain frequency standard in Japan with AIST. Since 2021, he has been with Platform Photonics Research Center with AIST. He is a Member of the Japan Society of Applied Physics and Physical Society of Japan.

Yasuhiro Ibusuki received the B.S. and M.S. degrees in electronics from the Tokyo Institute of Technology, Tokyo, Japan, in 1992 and 1994, respectively. In 1994, he joined Furukawa Electric Co., where he has been engaged with the research and development of optical components. Since 2016, he has been with the Photonics Electronics Technology Research Association, Tsukuba, Japan.

Akihiro Noriki received the B.S., M.S., and Ph.D. degrees in bioengineering and robotics from Tohoku University, Sendai, Japan, in 2008, 2010, and 2013, respectively. From 2013 to 2014, he was with the Graduate School of Biomedical Engineering, Tohoku University, where he studied 3-D stacked opto-electronic large-scale integration (LSIs) as a Research Fellow with the Japan Society for the Promotion of Science. Since 2014, he was with the National Institute of Advanced Industrial Science and Technology, Tsukuba, Japan. His research interests include optical I/O devices and packaging technologies for silicon photonics. Noriki is a Member of the Japan Society of Applied Physics.

Akio Ukita received the B.S. and M.S. degrees in electronics from the Tokyo Institute of Technology, Tokyo, Japan, in 1985 and 1987, respectively. In 1987, he joined NEC Co., where he engaged in production engineering research and development. Since 2012, he has been with the Photonics Electronics Technology Research Association.

Koichi Takemura (Member, IEEE) received the B.E. and M.E. degrees in metal science and technology from Kyoto University, Kyoto, Japan, in 1986 and 1988, respectively, and the D.E. degree in electronics and applied physics from the Tokyo Institute of Technology, Yokohama, Japan, in 2017. In 1988, he joined NEC Corporation, Kawasaki, Japan, and engaged in the research and development of high-dielectric-constant and ferroelectric thin-film capacitors for Gbit DRAMs, FeRAMs, and GaAs MMICs, and passive-embedded Si interposers for 3D system integration. From 1998 to 1999, he was a Visiting Researcher with Pennsylvania State University, State College, PA, USA. He was with the Association of Super-Advanced Electronics Technologies (ASET) from 2008 to 2010 and the Photonics Electronics Technology Research Association (PETRA) from 2012 to 2021. He is currently a General Manager (optical packaging) with AIO Core Co., Ltd., Tokyo, Japan. Dr. Takemura is a Member of IEEE Electronics Packaging Society, Japan Institute of Electronics Packaging, and Japan Society of Applied Physics.

Tsuyoshi Aoki received the B.E. and M.E. degrees in material engineering from Kyoto University, Kyoto, Japan, in 1998 and 2000, respectively, and the D.E. degree in material engineering from the University of Tokyo in 2005. In 2000, he joined Fujitsu Laboratories, Ltd., and has been engaged in the research and development of ferroelectric thin-film devices, optical multifiber connectors, and optical fiber assemblies. Since 2015, he has been participated in the Photonics Electronics Technology Research Association (PETRA) and has worked on silicon photonic optical engines and optical packaging technologies. He is also a Member of the Japan Institute of Electronics Packaging.

Takeru Amano was born in Tokyo, Japan on July 26, 1976. He received the B.E., M.E., and Ph.D. degrees from the Tokyo Institute of Technology, Tokyo, Japan, in 1999, 2001, and 2004, respectively. During his PhD studies, he worked on microelectromechanical systems, optical filters, and MEMS vertical cavity surface-emitting lasers. In 2004, he joined the Photonics Research Center, AIST as a Research Member. He is currently conducting research on quantum dot fabrication, quantum dot devices, and optical–electrical hybrid LSI packaging substrates. Dr. Amano was the recipient of IEEE LEOS Student Paper Award in 2000 and IEEE EDS Student Paper Award in 2002.